

# Online Object-Oriented Semantic Mapping and Map Updating with Modular Representations

Nils Dengler

Tobias Zaenker

Francesco Verdoja

Maren Bennewitz

**Abstract**—Creating and maintaining an accurate representation of the environment is an essential capability for every service robot. Especially semantic information is important for household robots acting in indoor environments. In this paper, we present a semantic mapping framework with modular map representations. Our system is capable of online mapping and object updating given object detections from RGB-D data and provides various 2D and 3D representations of the mapped objects. To undo wrong data association, we perform a refinement step when updating object shapes. Furthermore, we maintain a likelihood for each object to deal with false positive and false negative detections and keep the map updated. Our mapping system is highly efficient and achieves a run time of more than 10 Hz. We evaluated our approach in various environments using two different robots, i.e., a HSR by Toyota and a Care-O-Bot-4 by Fraunhofer. As the experimental results demonstrate, our system is able to generate maps that are close to the ground truth and outperforms an existing approach in terms of intersection over union, different distance metrics, and the number of correct object mappings. We plan to publish the code of our system for the final submission.

## I. INTRODUCTION

In any mobile robotics application, maps are of great importance. While geometrical map representations such as grid maps are an established researched topic, the research on mapping also semantic information becomes more and more popular. Especially for service robots, a proper environment understanding is necessary to not only navigate but also interact reasonably with the world. To generate accurate semantic maps for navigation, most research concentrates on object-based SLAM algorithms [1] or the complete 3D reconstruction of the world with semantic annotations [2]. However, the interest of maps with focus on just the objects has increased noticeably [3]–[7]. One of the main reasons is the usefulness of concrete object instances, which can be accessed more easily in an object-based approach. Most current approaches that create object-oriented maps have in common that they provide a 3D object reconstruction together with the position in the map. While the 3D information is necessary for any kind of manipulation, it can be considered as an overhead for navigation tasks considering object information [8].

In our approach, we maintain for each object instance multiple object information to address different applications.

N. Dengler, T. Zaenker, and M. Bennewitz are with the Humanoid Robots Lab, University of Bonn, Germany. F. Verdoja is with School of Electrical Engineering, Aalto University, Finland. This work has been partially funded by the Deutsche Forschungsgemeinschaft (DFG, German Research Foundation) under Germany's Excellence Strategy – EXC 2070 – 390732324 (PhenoRob) and by the Academy of Finland Strategic Research Council grant 314180.

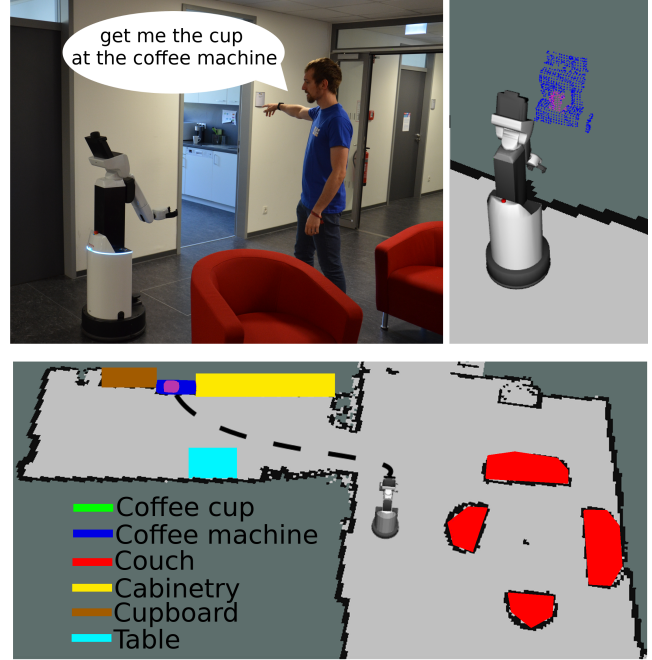


Fig. 1: Example usecase of our proposed system. A user commands the robot to get a specific cup (upper left image). To get the position of the cup, the robot checks the created map for cups near a coffee machine. The lower image shows a 2D polygonal representation of the environment mapped with our framework. With the 2D information, the robot can navigate to the goal destination. To grab the cup, the robot then utilizes the 3D representation of the objects (upper right image), which is also maintained by our system.

Apart from the 3D point cloud describing the object and its semantic type, also the 2D shape in form of a polygon and an oriented bounding box are stored. This allows the robot to increase or decrease the dimension of information according to the current task and the information is reduced to the relevant parts. A possible application of our system is shown in Fig. 1. Using the map created by our framework, the robot is able to identify the cup by checking for all cups close to a coffee machine. The robot can then navigate to the cup according to the mapped 2D shapes. For grabbing the cup, the 2D shape is not sufficient anymore and the robot can use the 3D point cloud representation.

For the mapping process, we assume that the 2D grid map and the robot pose are known. As in other approaches, we combine instance-level segmentation with a fast geometric segmentation to reconstruct objects from the incoming RGB-D data. To be able to keep the map updated in case of changes in the environment, we developed a data association

that is able to update mapped objects with newly collected object information. Our data association is hereby able to handle wrong object updates due to false segmentation. Furthermore, existing approaches update the map only if an object is detected, which can lead to a wrong representation due to removed or displaced objects. To counter this, we introduce an object-wise likelihood that is also updated for mapped objects not detected in the current field of view.

To sum up, in this paper we present a novel modular semantic mapping system with the following contributions:

- A map representation that provides several object information such as the object label, the point cloud, and two different 2D object shapes,
- A robust data association that is able to undo wrong object updates,
- A likelihood calculation for each mapped object to deal with false detections and keep the map updated,
- An experimental evaluation of our system in three different environments that shows the qualitative performance as well as the superior performance in comparison to Zaenker *et al.* [5] with respect to different metrics.

## II. RELATED WORK

Semantic maps describe the environment by assigning labels to detected features, which can be either objects [9]–[11] or more abstract places in the environment [4], [12]–[14]. The application areas of semantic maps range from small indoor environments [15] to whole buildings [16] up to outdoor environments, e.g., streets or parks [17].

For many scenarios, semantic 2D maps are sufficient, e.g., for simple search and navigation tasks. For example, Regier *et al.* [8] proposed to label cells of a 2D gridmap with object information and corresponding navigation cost to overcome the obstacles. Leidner *et al.* [18] presented a semantic mapping approach to augment existing geometric 2D maps. The authors demonstrated the automatic annotation of sub spaces on the example of warehouse environments. The main difference to our approach is that these frameworks do not output single object instances, but only the labeled geometric 2D map.

The research on object-oriented semantic mapping has increased in the last few years. The five approaches closest to our work are [3]–[7], which all address the problem of providing concrete object information. Object-oriented mapping approaches can be generally separated into two main parts, the applied object instance segmentation and the geometric segmentation. For the object instance segmentation, two variants are mainly used. In several approaches, mask R-CNNs [19] are applied to get an accurate instance mask of the detected objects [4], [5], [7]. Other approaches use detectors that provide only bounding boxes [3], [6]. The most popular ones are object detectors such as YOLO [20], the TensorFlow object detection API [21], and single shot detectors [22], which provide many pretrained models that can be used off-the-shelf. For this reason, we use a pretrained faster R-CNN [23] from TensorFlow [21]. Note that it can be

replaced by, e.g., a mask R-CNN with just minor changes.

For the geometric segmentation, the research towards supervised methods has increased [24] [25]. However, those approaches need prior knowledge and training data. Our system, in contrast, does not need any prior knowledge about the object shape. In most approaches, the objects are already segmented in the depth image before computing the corresponding 3D points [3], [6], [7]. While there is no apparent benefit in computing the segments on the depth image and the point cloud has to be computed anyway, we carry out the segmentation on the point cloud. With a cluster computation time of less than 1 ms our approach is faster than, e.g., Sünderhauf *et al.* [3]. Li *et al.* [4] propose to apply a Gaussian mixture model [26] instead of geometric segmentation to refine the mapped object regions generated according to the segmentation masks.

While these approaches also generate object-oriented semantic maps as our system, there are three major benefits that are not addressed by the other works. All approaches have in common that they are restricted to represent the world in 3D. Since the map representation depends heavily on the task, our approach is not limited to just a 2D or 3D representation, but combines multiple variants in a modular way. A further benefit is that our approach performs a more robust data association and can fix possible wrong object matchings in the long run. Finally, we maintain a likelihood for each object. Typically, object-oriented approaches update the objects only if they are re-detected, as stated in [3]. That means that especially if the environment is non-static and objects change their location, the probability of misinterpreting the new object points as the old ones is quite high. In contrast, our proposed system is able to manage these changes and update the map even if the object is no longer present at its previous location.

Our semantic mapping framework is inspired by the hypermap framework proposed by Zaenker *et al.* [5] and improves it in several aspects. The main contribution of the hypermap is the combination of multiple maps in a single representation to simplify the communication between the robot and multiple maps. However, Zaenker *et al.* also presented an object-oriented semantic mapping system that, in contrast to our approach, only provides a 2D representation and completely ignores further object information. Furthermore, we apply different methods to improve major parts of [5] such as the object shape generation, the likelihood calculation, and the data association.

## III. OBJECT-ORIENTED SEMANTIC MAPPING

In this section, we describe the four main parts of our system. The semantic map generated by our approach consists of  $N$  so-called semantic objects  $o$ . To guarantee an easy access, we store all semantic objects  $o_1, \dots, o_N$  in a list. Each  $o_i$  is defined by several features such as the object type, the corresponding point cloud, the 2D shape polygon and oriented bounding box (OBB), as well as the 2D and 3D position, and the likelihood. The first part of our framework is the preprocessing and segmentation of the incoming point

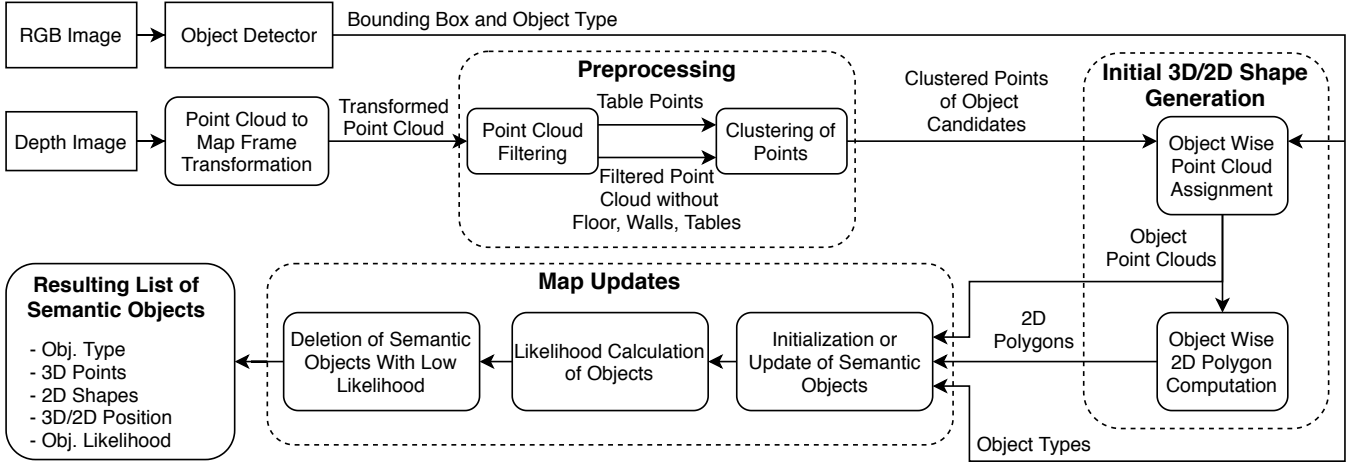


Fig. 2: Overview of our semantic mapping system. The squared boxes indicate the external inputs.

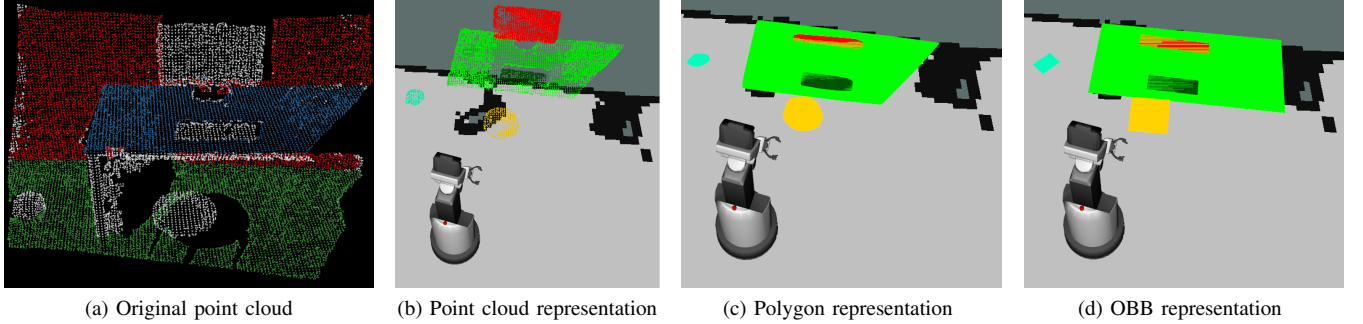


Fig. 3: Office working place, observed by the robot. (a) visualizes the whole incoming point cloud with the three filtered surfaces colored in red (wall), blue (table) and green (floor). All remaining parts of the point cloud after the preprocessing are colored white. Figures (b) to (d) show the mapped objects in three different representations (point cloud, polygon, and oriented bounding box (OBB)).

cloud. Then each segmented part is assigned to an detected object in the RGB image. Subsequently, our system checks whether the object can be associated to an already mapped semantic object, if not, the new objects is included into the semantic map. If an already existing semantic object is updated, the likelihood is re-calculated and used to remove or add objects. Fig. 2 shows an overview of our system. The individual steps are described in detail in the following.

#### A. Detection of Objects

In semantic mapping, the interest in using mask R-CNNs [19] as object detector to get more precise object instances has increased [4], [7]. However, a major restriction of current object detectors is the limited amount of classes in freely available pretrained nets. While the popular COCO dataset [27] can detect up to 80 different classes, important objects for office environments such as tables are missing. To show the performance of our system especially for smaller items, the small amount of object classes is not suitable. Therefore, we use a faster R-CNN trained on the OpenImages-Dataset [28]. This dataset includes more than 600 classes, with almost any object commonly seen in households or offices. Note that our framework is modular and the detection method is easily replaceable.

#### B. Point Cloud Preprocessing

An important step is the preprocessing of the transformed point cloud before the possible object clusters are computed. In a first step, our system removes the floor and the walls. To facilitate the segmentation of smaller objects on tabletops, they are also removed from the initial point cloud but the corresponding points are stored separately since tables are important semantic objects. We hereby apply the RANSAC algorithm [29]. After this filtering step, the remaining objects are better recognizable and easier to cluster, as illustrated in Fig. 3a. Furthermore, we perform a statistical outlier removal step to increase the accuracy of the point cloud and counter the assignment of wrong points before the geometric segmentation.

#### C. Geometric Segmentation

As next step, we apply geometric segmentation on the preprocessed point cloud. To perform the geometric segmentation, we apply the Euclidean cluster extraction of PCL [30]. Since it is easier for the algorithm to find larger clusters, due to more continuous information, we compute the clusters for the whole preprocessed point cloud instead of the cut object point clouds. Because there is a high probability to also have very small objects in the environment, e.g., cups

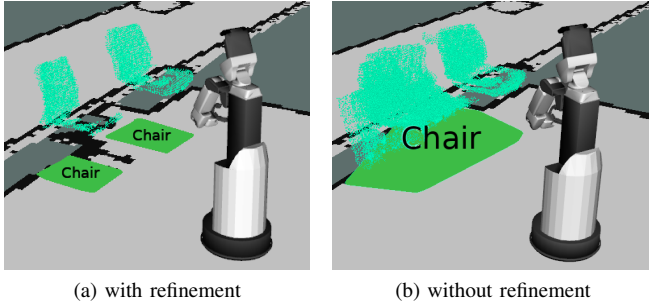


Fig. 4: Example of the mapping part of the environment (a) with and (b) without object shape refinement during updates. Shown are the object point cloud, the 2D polygons and the label. In (a) the two chairs are clearly separated, while in (b) they are merged together due to many outliers resulting from, e.g., wrong segmentation or localization inaccuracy.

or phones, we hereby use a minimum cluster size of 100 points, which that depends on the point cloud density. After the segmentation, we store the generated clusters to combine them with the bounding boxes of the object detector.

#### D. Initial 3D and 2D Object Shape Generation

Given the bounding box of each object and the generated clusters, our system assigns the best fitting cluster to each bounding box. To do so, it first determines the cluster that has the highest number of points inside the object bounding box. Afterwards, the corresponding points inside the box are stored as the object point cloud. To generate the initial 2D object shape, all 3D points of the object point cloud are projected onto the 2D  $x-y$ -plane and the convex hull of the remaining points is computed to express it as a polygon. As further 2D shape variant, we also compute the oriented bounding box (OBB) using the rotating calipers method [31]. In contrast to the polygon, the OBB can be a better approximation of the real shape if parts of an object are obscured. Fig. 3b-d show the representations of part of an office scene.

Furthermore, we determine the 2D and 3D position as the center of mass (CoM) of the corresponding representation.

#### E. Initialization and Update of Semantic Objects

Data association is a key element of every semantic mapping framework. To determine whether to insert a new object or update an existing  $o_i$  when processing a new detection, our system uses an R-tree structure [32] to find overlapping polygons of the same object type, which can be combined. The update process then consists of one of the following two cases.

*New object:* In the first case, the initial polygon has no intersection with any already mapped object and therefore our system creates a new semantic object.

*Association with at least one existing semantic object:* In the second case, the point clouds of all overlapping semantic objects are combined together with the newly found object to create a single semantic object. We hereby filter the combined point cloud with a voxel

grid to get evenly distributed points. As described in Section III-D, the polygon of the corresponding combined objects is updated as well as the OBB. While all previously combined objects are deleted from the R-tree, the updated object is newly included.

It is possible that in the update process wrong points are associated to an object, due to errors in the segmentation process or localization inaccuracies. In this case, there is a high probability that close-by objects of the same class are combined because of the expanded object shapes. To refine the object shape and ensure that multiple incorrectly combined objects can be separated again, our system calculates new Euclidean clusters of the object point cloud if an  $o_i$  was combined more than a predefined amount of times. If the algorithm finds more than one cluster in the point cloud of an  $o_i$ , the biggest cluster is assigned to the  $o_i$  and new semantic objects are created for the other clusters. Fig. 4 shows the mapping of two chairs with and without the object refinement. Without the object refinement points from other structures are included in the point cloud, which wrongly extends the shape. Furthermore, points of the other chair intersect with the first one and lead to the combination of the two objects. With the refinement, the objects are separated and have clean boundaries.

#### F. Object Likelihood

To keep the map updated in case of object displacements or removals as well as to deal with false detections, object deletion is an important property of our system. In other frameworks such as [3], the map is only updated wrt. the semantics if the object is re-observed and in case an object is removed or displaced by another object, the semantic object instance remains in the map. To counter this problem, we calculate a likelihood for the existence of each semantic object each time the object should be in the field of view (FoV), i.e., our system counts the number of times an object was initialized or updated (hit) or not (miss). After each iteration, our system updates the likelihood of object  $i$  as follows:

$$L_i = \frac{hits_i}{\frac{1}{hit_i + misses_i} + misses_i + hits_i} \quad (1)$$

The higher the likelihood, the higher the confidence that the object really exists. With the term  $\frac{1}{hit_i + misses_i}$  we achieve a smooth likelihood evolution and keep some uncertainty for the objects. To delete objects from the map, we use a threshold  $\tau$ . If  $L_i < \tau$ , the corresponding semantic object will be deleted. As a constraint, the summed up maximum amount of hits and misses is limited to a predefined number so that it cannot grow infinitely and detections far in the past are not weighted. To accomplish this, the oldest detection is deleted and the newest one is added. Furthermore, we consider a minimum number of summed up hits and misses to encounter the inconsistency of the object detector and ensure that early false negative detections will not affect the mapping, such that the object is removed although it is still in the environment.



### G. Map Generation

The list of all  $o_i$  defines the semantic map and allows to address each  $o_i$  and access the information stored in it at any time. Since the visualization of the map can also be of great importance for certain tasks, we extended the Rviz display by Zaenker *et al.* [5] to visualize the collected map information. In this display, the user can decide to show either the polygon, the OBB, the point cloud, or the label of each object, but also all of those at the same time.

## IV. EXPERIMENTAL EVALUATION

We evaluated our approach on a computer with an i9-9900K eight-core CPU at 3.60 GHz and an Nvidia 2080 GPU with 8 GB of memory used for the faster R-CNN. The object detection framework is based on the implementation of [21] and we used it with weights pretrained on the OpenImagesV4 dataset [28]. As base mapping and localization methods we deploy the ROS implementations of the *gmapping* SLAM algorithm [33] and the Monte Carlo localizer [34]. In the following, we first evaluate the online mapping capability of our system in different environments and compare it to the approach of Zaenker *et al.* [5]. Then we demonstrate the evolution of the object likelihood values and, finally, analyze the runtime. The accompanying video shows the performance of our approach in several real-world experiments.

### A. Online Object Mapping and Map Updates

To show the performance of our system, we carried out four experiments in three different real-world environments. For the first three experiments, we used the HSR by Toyota [35] to record the RGB-D data collected with an Asus Xtion Pro mounted at a height of 1.35m and in an angle of 36° from the horizontal facing down. The last experiment was carried out with the Care-O-Bot-4 by Fraunhofer [36], with an Asus Xtion Pro mounted at a height of 1.02m horizontal to the floor. We used a resolution of 640x480 pixels for the cameras.

The first environment is an office environment of 29m<sup>2</sup> with several usual and unusual office items. To evaluate the update capability of our system, we split the experiment in the office environment into two parts. In the second part of the experiment, some objects in the room were displaced, exchanged, removed, or newly added. The second environment is with 60m<sup>2</sup> twice as large and consists of a kitchen as well as a sofa corner as shown in Fig 1. The third environment is a coffee room of 35m<sup>2</sup> in the Aalto University. This environment was much more cluttered than the office environment and therefore more challenging.

We evaluated our approach on the four sequences in comparison to the hypermap (H-Map) framework by Zaenker *et al.* [5]. For each experiment and each approach, we computed the average intersection over union (IoU), Hausdorff-distance (H-dist), distance to the 2D center of mass (CoM), and the number of true positive (TP) as well as false positive (FP) object mappings. Note that the handcrafted ground truth map (see Fig 5a) is only an approximation of the real world. A further factor that influences

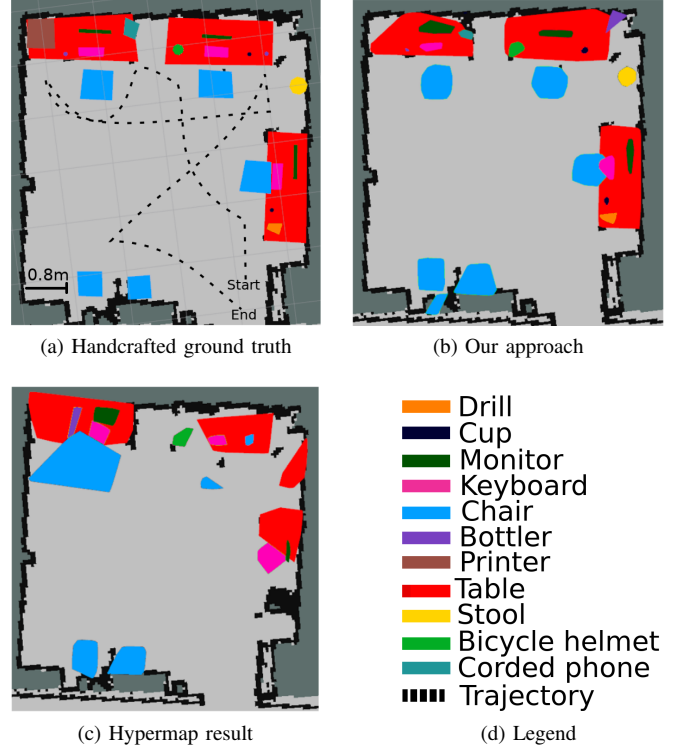


Fig. 5: (a) Visualization of the handcrafted ground truth map, (b) result of the presented approach, and (c) result of the approach by Zaenker *et al.* [5]. Each object is represented by a polygon, colored corresponding to the object class shown in (d). While our approach achieves a result close to the ground truth, the hypermap is just a rough approximation.

the results of both approaches is the localization accuracy, which changes over time. Both approaches were evaluated under the same conditions. The results in Table I show that our approach outperforms the H-Map in all but the number of FPs. We explain the higher FP values with the added objects by the object refinement. An example of this can be seen around the lower two chairs in Fig. 5b, where an additional shape was added due to the object refinement. Note that the likelihood value of all FPs was lower than 0.5 and the corresponding wrongly mapped objects would disappear with more observations. For our experiments, we defined a maximum of 30 observations and a deletion threshold of 0.25.

To see whether the differences between the results of the metrics are significant, we used the one-sided Wilcoxon sign rank test. The difference of the results marked with a \* in Tab. I are significant with a chosen p-value of 0.05. By looking at the resulting maps shown in Fig. 5 the difference between our approach and the H-Map is clearly visible. Especially, the objects on the tablespots and the chairs are better approximated and close to the ground truth.

### B. Evolution of the Object Likelihood

To show the strength of the object update with likelihood values, we recorded a sequence with changing chair and table appearances over time. Fig. 6 shows the evolution of

Office 1	IoU*	H-Dist*	CoM-Dist*	TP	FP
Polygon	0.58 $\pm$ 0.16	0.12m $\pm$ 0.05	0.04m $\pm$ 0.02	20/23	4
Obb	0.51 $\pm$ 0.18	0.14m $\pm$ 0.06	0.04m $\pm$ 0.02	20/23	4
H-map [5]	0.35 $\pm$ 0.18	0.44m $\pm$ 0.24	0.21m $\pm$ 0.11	16/23	1

Large	IoU*	H-Dist*	CoM-Dist*	TP	FP
Polygon	0.49 $\pm$ 0.15	0.24m $\pm$ 0.15	0.09m $\pm$ 0.06	25/33	8
Obb	0.44 $\pm$ 0.16	0.27m $\pm$ 0.16	0.10m $\pm$ 0.08	25/33	8
H-map [5]	0.26 $\pm$ 0.12	0.53m $\pm$ 0.17	0.25m $\pm$ 0.10	18/34	1

Office 2	IoU*	H-Dist*	CoM-Dist*	TP	FP
Polygon	0.51 $\pm$ 0.18	0.17m $\pm$ 0.12	0.08m $\pm$ 0.05	21/23	10
Obb	0.45 $\pm$ 0.18	0.18m $\pm$ 0.13	0.08m $\pm$ 0.06	21/23	10
H-map [5]	0.29 $\pm$ 0.15	0.55m $\pm$ 0.44	0.27m $\pm$ 0.23	18/23	8

Cluttered	IoU	H-Dist	CoM-Dist	TP	FP
Polygon	0.29 $\pm$ 0.19	0.45m $\pm$ 0.30	0.21m $\pm$ 0.21	19/33	8
Obb	0.29 $\pm$ 0.21	0.48m $\pm$ 0.33	0.21m $\pm$ 0.21	19/33	8
H-map [5]	0.16 $\pm$ 0.09	0.76m $\pm$ 0.49	0.38m $\pm$ 0.24	14/33	4

TABLE I: Quantitative evaluation with respect to the average intersection over union (IoU), center of mass distance (CoM-Dist), Hausdorff distance (H-Dist), as well as the number of true positive (TP) and false positive (FP) object mappings. Also the standard deviation of each metric is shown. The results are in comparison to the hypermap framework by Zaenker *et al.* [5] where the metrics marked with a \* are significant according to the Wilcoxon sign rank test. As can be seen our approach outperform the hypermap in all but the FPs. We explain the higher FP values with the added objects by the object refinement. with more observations this value will decrease.

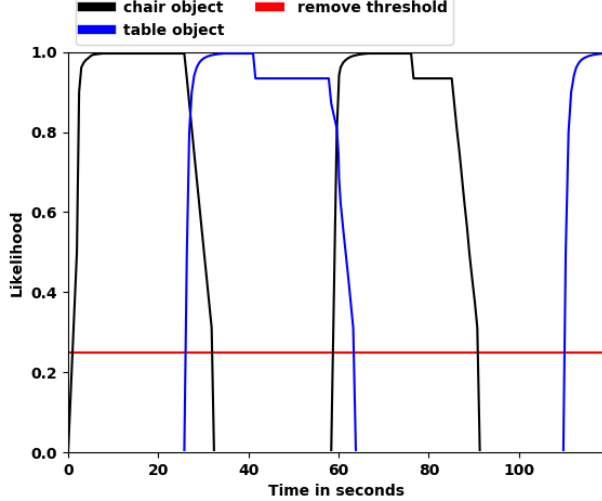


Fig. 6: Likelihood evolution over time for two different object types. The likelihood grows as long as the object is detected and decreases otherwise. If the mapped object is not in the robot's field of view the likelihood remains static. The red line shows the threshold of deleting an object from the map.

the likelihood values. While the robot observes the object, the likelihood grows constantly until it reaches a value of nearly 1. As long as the robot's camera view does not cover the position of the mapped object, the likelihood is not updated. If the mapped object is not detected anymore within the FOV, the likelihood decreases and the object is removed as soon as it reaches the predefined threshold of 0.25. In this experiment, we displaced the objects in the scene while they were not in the robot's FOV. That is why a small time window exists where both objects are mapped. The required time to remove an unseen object from the map depends on the predefined deletion threshold and the maximum number of observations that are considered for the likelihood calculation. In the first mapping of the table, the result of an unstable object detection can be seen. As soon as the robot turns away, it no longer detects the object and therefore the likelihood decreases until the value remains stable when the object is no longer in the FOV. As this example demonstrates, our system is able to keep the map updated in case object locations change and can also deal with false detections.

Component	Avg time
Point cloud transformation	7 ms
Preprocessing	31 ms
Euclidean segmentation	0.01 ms
Data association and object updates *	11 ms
Likelihood computation and object deletion	2 ms
Complete average run time per frame	85 ms
Faster R-CNN	425 ms

TABLE II: Average run time per frame of the main components of our system and the complete run time for a dataset of the office environment. The run time of the component marked with a \* is the average computation time for one object. All components are included in the 85 ms. Note that the output of faster R-CNN can be computed parallel to our system. The run time of the object detector depends on the used network and is not included in the overall run time of our system.

### C. Run Time Evaluation

To show that our system is capable of online mapping, we also evaluated the run time. To measure the time of each component, we used the data set of the office environment. We recorded the experiment over a length of 6.36 minutes and up to 33 mapped objects. The resulting time, shown in Table II is the average computation time per frame over the whole data set. It can be seen that the overall run-time of the office environment is 85 ms (11.76 Hz). Most of the time is taken by the outlier removal in the preprocessing and by each object update, which can vary depending on the number of mapped objects and the size of the point cloud. The resulting computation time demonstrates the online mapping capability of our system and the increased runtime performance in comparison to the approaches by Sünderhauf *et al.* [3] and Li *et al.* [4].

## V. CONCLUSION

In this paper, we presented an approach to online semantic mapping with modular object representations. Our approach differs from previous work in the way the created map is represented so that it is not restricted to just one representation but maintains multiple of representations within one framework. Furthermore, the introduced likelihood calculation of each object is a way to keep the map updated in case objects change their location and achieve robustness in case of false detections. Our object refinement step ensures that object point assignments can be undone to deal with wrong data association. We demonstrated the efficacy of our approach in four real-world experiments where the results show the increased performance in comparison to an existing

framework with respect to different metrics. The evaluation of the runtime highlights that our system is able of online mapping while the robot is moving through the environment. In the future, we plan to integrate our approach with the work of Bruckschen *et al.* [37] that combines multiple objects to activity regions and uses them for predicting user activities.

## REFERENCES

- [1] C. Cadena, L. Carlone, H. Carrillo, Y. Latif, D. Scaramuzza, J. Neira, I. Reid, and J. J. Leonard, "Past, Present, and Future of Simultaneous Localization And Mapping: Towards the Robust-Perception Age," *IEEE Transactions on robotics*, vol. 32, no. 6, pp. 1309–1332, 2016.
- [2] A. Rosinol, M. Abate, Y. Chang, and L. Carlone, "Kimera: an Open-Source Library for Real-Time Metric-Semantic Localization and Mapping," in *Proc. of the IEEE Intl. Conf. on Robotics & Automation (ICRA)*, 2020, pp. 1689–1696.
- [3] N. Sünderhauf, T. T. Pham, Y. Latif, M. Milford, and I. Reid, "Meaningful Maps With Object-Oriented Semantic Mapping," in *Proc. of the IEEE/RSJ Intl. Conf. on Intelligent Robots and Systems (IROS)*, 2017, pp. 5079–5085.
- [4] W. Li, J. Gu, B. Chen, and J. Han, "Incremental Instance-Oriented 3D Semantic Mapping via RGB-D Cameras for Unknown Indoor Scene," *Discrete Dynamics in Nature and Society*, vol. 2020, 2020.
- [5] T. Zaenker, F. Verdoja, and V. Kyrki, "Hypermap Mapping Framework and its Application to Autonomous Semantic Exploration," in *Proc. of the IEEE Conference on Multisensor Fusion and Integration (MFI)*, 2020.
- [6] Y. Nakajima and H. Saito, "Efficient Object-Oriented Semantic Mapping With Object Detector," *IEEE Access*, vol. 7, pp. 3206–3213, 2018.
- [7] M. Grinvald, F. Furrer, T. Novkovic, J. J. Chung, C. Cadena, R. Siegwart, and J. Nieto, "Volumetric Instance-Aware Semantic Mapping and 3D Object Discovery," *IEEE Robotics and Automation Letters (RA-L)*, vol. 4, no. 3, pp. 3037–3044, July 2019.
- [8] P. Regier, A. Milioto, C. Stachniss, and M. Bennewitz, "Classifying Obstacles and Exploiting Class Information for Humanoid Navigation Through Cluttered Environments," *The Int. Journal of Humanoid Robotics (IJHR)*, vol. 17, no. 2, pp. 2050013–1, 2020.
- [9] A. J. Trevor, S. Gedikli, R. B. Rusu, and H. I. Christensen, "Efficient Organized Point Cloud Segmentation with Connected Components," *Semantic Perception Mapping and Exploration (SPME)*, 2013.
- [10] G. Narita, T. Seno, T. Ishikawa, and Y. Kaji, "PanopticFusion: Online Volumetric Semantic Mapping at the Level of Stuff and Things," *arXiv preprint*, 2019.
- [11] S. Zhi, M. Bloesch, S. Leutenegger, and A. J. Davison, "Scenecode: Monocular Dense Semantic Reconstruction using Learned Encoded Scene Representations," in *Proc. of the IEEE Conf. on Computer Vision and Pattern Recognition (CVPR)*, 2019, pp. 11 776–11 785.
- [12] Z. Liu, D. Chen, and G. von Wichert, "2D Semantic Mapping on Occupancy Grids," in *ROBOTIK 2012; 7th German Conference on Robotics*. VDE, 2012, pp. 1–6.
- [13] G. Costante, T. A. Ciarfuglia, P. Valigi, and E. Ricci, "A Transfer Learning Approach for Multi-Cue Semantic Place Recognition," in *Proc. of the IEEE/RSJ Intl. Conf. on Intelligent Robots and Systems (IROS)*, 2013, pp. 2122–2129.
- [14] X. Hu, H. Fan, A. Nodkov, Z. Wang, A. Zipf, F. Gu, and J. Shang, "Room semantics inference using random forest and relational graph convolutional networks: A case study of research building," *Transactions in GIS*, 2020.
- [15] A. Hermans, G. Floros, and B. Leibe, "Dense 3D Semantic Mapping of Indoor Scenes from RGB-D Images," in *Proc. of the IEEE Intl. Conf. on Robotics & Automation (ICRA)*, 2014, pp. 2631–2638.
- [16] A. Pronobis and P. Jensfelt, "Large-Scale Semantic Mapping and Reasoning with Heterogeneous Modalities," in *Proc. of the IEEE Intl. Conf. on Robotics & Automation (ICRA)*, 2012, pp. 3515–3522.
- [17] F. Bernuy and J. Ruiz del Solar, "Semantic Mapping of Large-Scale Outdoor Scenes for Autonomous Off-Road Driving," in *Proc. of the IEEE Intl. Conf. on Computer Vision Workshops (ICCV)*, 2015, pp. 35–41.
- [18] D. Leidner, A. Dietrich, F. Schmidt, C. Borst, and A. Albu-Schäffer, "Object-Centered Hybrid Reasoning for Whole-Body Mobile Manipulation," in *Proc. of the IEEE Intl. Conf. on Robotics & Automation (ICRA)*, 2014, pp. 1828–1835.
- [19] K. He, G. Gkioxari, P. Dollár, and R. Girshick, "Mask r-cnn," in *Proc. of the IEEE Intl. Conf. on Computer Vision (ICCV)*, 2017, pp. 2961–2969.
- [20] J. Redmon, S. Divvala, R. Girshick, and A. Farhadi, "You Only Look Once: Unified, Real-Time Object Detection," in *Proc. of the IEEE Conf. on Computer Vision and Pattern Recognition (CVPR)*, 2016, pp. 779–788.
- [21] "Tensorflow object detection," <https://github.com/osrf/tensorflow-object-detector>, last accessed 29. June 2020.
- [22] W. Liu, D. Anguelov, D. Erhan, C. Szegedy, S. Reed, C.-Y. Fu, and A. C. Berg, "SSD: Single Shot Multibox Detector," in *Proc. of the Europ. Conf. on Computer Vision (ECCV)*. Springer, 2016, pp. 21–37.
- [23] S. Ren, K. He, R. Girshick, and J. Sun, "Faster R-CNN: Towards Real-Time Object Detection with Region Proposal Networks," in *Advances in neural information processing systems*, 2015, pp. 91–99.
- [24] R. A. Rosu, J. Quenzel, and S. Behnke, "Semi-Supervised Semantic Mapping through Label Propagation with Semantic Texture Meshes," *Intl. Journal of Computer Vision (IJCV)*, vol. 128, no. 5, pp. 1220–1238, 2020.
- [25] S. Stekovic, F. Fraundorfer, and V. Lepetit, "Casting Geometric Constraints in Semantic Segmentation as Semi-Supervised Learning," in *Proc. of the IEEE Winter Conference on Applications of Computer Vision (WACV)*, 2020, pp. 1854–1863.
- [26] B. G. Lindsay, "Mixture models: Theory, geometry and applications," in *NSF-CBMS regional conference series in probability and statistics*. JSTOR, 1995, pp. i–163.
- [27] T.-Y. Lin, M. Maire, S. Belongie, J. Hays, P. Perona, D. Ramanan, P. Dollár, and C. L. Zitnick, "Microsoft COCO: Common Objects in Context," in *Proc. of the Europ. Conf. on Computer Vision (ECCV)*. Springer, 2014, pp. 740–755.
- [28] I. Krasin, T. Duerig, N. Alldrin, V. Ferrari, S. Abu-El-Hajja, A. Kuznetsova, H. Rom, J. Uijlings, S. Popov, S. Kamali, M. Mallocci, J. Pont-Tuset, A. Veit, S. Belongie, V. Gomes, A. Gupta, C. Sun, G. Chechik, D. Cai, Z. Feng, D. Narayanan, and K. Murphy, "Openimages: A public dataset for large-scale multi-label and multi-class image classification." *Dataset available from <https://storage.googleapis.com/openimages/web/index.html>*, 2017.
- [29] M. A. Fischler and R. C. Bolles, "Random Sample Consensus: A Paradigm for Model Fitting with Applications to Image Analysis and Automated Cartography," *Communications of the ACM*, vol. 24, no. 6, pp. 381–395, 1981.
- [30] R. B. Rusu and S. Cousins, "3D is here: Point Cloud Library (PCL)," in *Proc. of the IEEE Intl. Conf. on Robotics & Automation (ICRA)*, Shanghai, China, May 9–13 2011.
- [31] H. Freeman and R. Shapira, "Determining the Minimum-Area Encasing Rectangle for an Arbitrary Closed Curve," *Communications of the ACM*, vol. 18, no. 7, pp. 409–413, 1975.
- [32] A. Guttman, "R-Trees: A Dynamic Index Structure for Spatial Searching," in *Proc. of the ACM SIGMOD international conference on Management of data (MOD)*, 1984, pp. 47–57.
- [33] G. Grisetti, C. Stachniss, and W. Burgard, "Improved Techniques for Grid Mapping with Rao-Blackwellized Particle Filters," *IEEE transactions on Robotics*, vol. 23, no. 1, pp. 34–46, 2007.
- [34] D. Fox, W. Burgard, F. Dellaert, and S. Thrun, "Monte Carlo Localization: Efficient Position Estimation for Mobile Robots," *aaai*, vol. 1999, no. 343–349, pp. 2–2, 1999.
- [35] T. Yamamoto, T. Nishino, H. Kajima, M. Ohta, and K. Ikeda, "Human Support Robot (HSR)," in *ACM SIGGRAPH emerging technologies*, 2018, pp. 1–2.
- [36] R. Kittmann, T. Fröhlich, J. Schäfer, U. Reiser, F. Weißhardt, and A. Haug, "Let me introduce myself: I am care-o-bot 4, a gentleman robot," *Proc. of Mensch und computer (MUC)*, 2015.
- [37] L. Bruckschen, K. Bungert, N. Dengler, and M. Bennewitz, "Predicting Human Navigation Goals Based on Bayesian Inference and Activity Regions," *Journal on Robotics and Autonomous Systems (RAS)*, 2020.